Giant Spin-Orbit Torque in Graphene–Topological-Insulator Heterostructures

M. Rodriguez-Vega,[1] G. Schwiete,[2] J. Sinova,[3, 4] and E. Rossi[1]

[1]*Department of Physics, College of William and Mary, Williamsburg, VA 23187, USA*
[2]*Department of Physics and Astronomy, Center for Materials for Information Technology (MINT),*
The University of Alabama, Alabama 35487, USA
[3] *Institut für Physik, Johannes Gutenberg Universitat Mainz, 55128 Mainz, Germany.*
[4]*Institute of Physics, Academy of Sciences of the Czech Republic,*
Cukrovarnicka 10, 162 53 Praha 6 Czech Republic
(Dated: June 9, 2017)

The control of a ferromagnet's magnetization via only electric currents requires the efficient generation of current-driven spin-torques. In magnetic structures based on topological insulators (TIs) current-induced spin-orbit torques can be generated. Here we show that the addition of graphene, or bilayer graphene, to a TI-based magnetic structure greatly enhances the current-induced spin-orbit torques and significantly reduces the amount of power dissipated. We find that this enhancement can be as high as a factor of 100, giving rise to a giant spin-orbit torque. Such a large enhancement is due to the high mobility of graphene (bilayer graphene) and to the fact that the graphene (bilayer graphene) sheet very effectively screens charge impurities, the dominant source of disorder in topological insulators. Our results show that the integration of graphene in spintronics devices can greatly enhance their performance and functionalities.

PACS numbers:

The ability to generate and control spin currents in condensed matter systems has led to several discoveries of great fundamental and technological interest [1, 2]. In recent years the discovery of whole new classes of materials with strong spin-orbit coupling, such as topological insulators (TIs) [3, 4], has allowed the realization of novel basic spin-based phenomena [5–8].

In a system with spin-orbit coupling (SOC), a charge current (I) can induce a spin-Hall effect (SHE) [2] i.e. a pure spin-polarized current. A companion effect to the SHE, also arising from the SOC, is the inverse spin-galvanic effect (ISGE), where a current induces a non-equilibrium uniform spin accumulation [2, 9–11]. In a magnetic system this current-driven spin accumulation results in a spin-orbit torque (SOT) acting on the magnetization (**M**), and therefore can be exploited to realize current-driven magnetization dynamics. The SOT, $\boldsymbol{\tau}_{SO}$, can be either an (anti-)damping torque [2, 12], i.e. have the same functional form as the Gilbert damping term, or *field-like* [2], i.e. have the form $\boldsymbol{\tau}_{SO} = \gamma \mathbf{B}_{SO} \times \mathbf{M}$, where $\mathbf{B}_{SO}$ is an effective spin-orbit field, and γ is the gyro-magnetic ratio. The presence of a current-driven SOT on the surface of TIs has been predicted [13–16] and it has been recently measured in TI-ferromagnet bilayers [17] and magnetically doped TIs [18].

The two-dimensional nature of graphene and bilayer graphene (BLG) [19–21] and the fact that their room-temperature mobilities are higher than in any other known material [22] make them extremely interesting for transport phenomena. However, the SOC in graphene is extremely small and as a consequence graphene alone is not very interesting for spintronics applications, except as a spin-conductor. Recent experiments on graphene-TI heterostructures seem to demonstrate the injection of

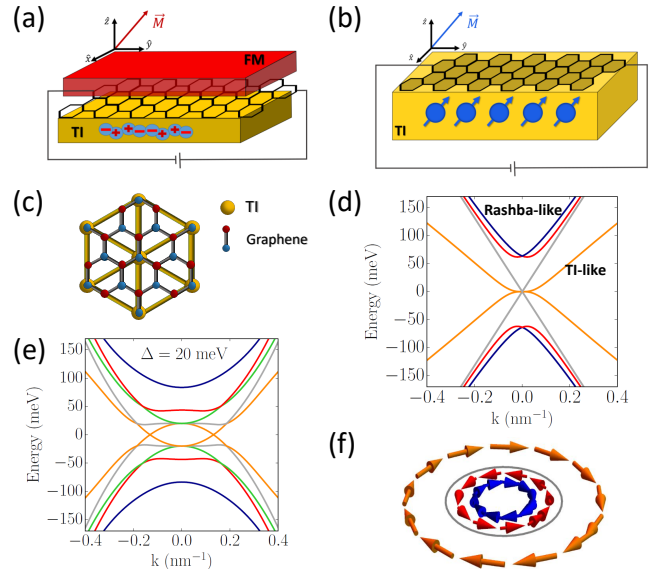spin-polarized current from a TI into graphene [23, 24].

FIG. 1: Sketch of a TI-graphene-FM, (a), and of a magnetically doped TI-graphene, (b), heterostructure. In (a) the random charges are shown. In (b) the spheres represent magnetic dopant, the random charges are not shown explicitly. (c) Atoms' arrangement for the commensurate stacking considered. (d) Bands for TI-SLG for $\Delta = 0$, $\delta\mu = 0$. (e) Bands for TI-BLG for $\Delta = 20$ meV and $\delta\mu = 0$. (f) Spin texture on the Fermi surface formed by the bands shown in (d) for $\epsilon_F = 100$ meV.

In this work we show that the combination of a particular class of three-dimensional (3D) TIs and graphene allows the realization of devices in which a charge current induces a SOT that can be up to a factor 100 larger

than in any previous system, i.e. a *giant SOT*. We find that for most of the experimentally relevant conditions considered the SOT in TI-graphene vdW heterostructures should be higher than the already very large values observed in TI-Ferromagnet bilayers [17] and magnetically doped TIs [18]. In Ref. 17, for $I = 7.7$ mA, a $B_{SO} = 3 \times 10^{-2}$ mT was measured, in Ref. 18, for $I = 4\mu$A, a $B_{SO} = 80$ mT was measured [25]. Assuming that our work is able to capture the key elements affecting the SOT in TI-graphene systems we find that in these systems the SOT could be ten times larger than the values found in Ref. 17, 18. We also find that TI-SLG and TI-BLG systems have conductivities much higher than TI surfaces and would therefore allow the realization of spintronics effects with dramatically lower dissipation than in TIs alone.

In vdW heterostructures [26], the different layers are held together by vdW forces. This fact greatly enhances the type of heterostructures that can be created given that the stacking is not fixed by the chemistry of the elements forming the heterostructure. With $a = 2.46\text{\AA}$ being the lattice constant of graphene, and a_{TI} the lattice constant of the 111 surface of a TI in the tetradymite family, we have $a_{TI}/a = \sqrt{3}(1+\delta)$, where $\delta < 1\%$ for Sb_2Te_3, $\delta = -3\%$ for Bi_2Se_3, and $\delta = 3\%$ for Bi_2Te_3. As a consequence, graphene and the 111 surface of Sb_2Te_3, Bi_2Se_3, Bi_2Te_3, to very good approximation, can be arranged in a $\sqrt{3} \times \sqrt{3}$ commensurate pattern [4, 27, 28]. When the stacking is commensurate the hybridization between the graphene's and the TI's surface states is maximized. This property of graphene, combined with its high mobility, its intrinsic two-dimensional nature, and its ability at finite dopings to effectively screen the dominant source of disorder in TIs, make graphene the ideal material to consider for creating a TI heterostructure with a very large SOT.

TI-graphene heterostructures can be formed via mechanical transfer [24, 30, 31] and as a consequence the stacking pattern, and the shift in particular, is fixed by the exfoliation-deposition process and can be controlled [32]. Density functional theory (DFT) results show [27, 33, 34] that the binding energy between graphene and the TI's surface depends only very weakly on the rigid shift. For concreteness in the remainder we consider the stacking shown in Fig. 1 (c).

At low energies, the Hamiltonian for the system can be written as $H = \sum_{\mathbf{k}} \psi_{\mathbf{k}}^{\dagger} H_{\mathbf{k}} \psi_{\mathbf{k}}$ where $\psi_{\mathbf{k}}^{\dagger}$ ($\psi_{\mathbf{k}}$) is the creation (annihilation) spinor for a fermionic excitation with momentum $\mathbf{k}$, and

$$\mathrm{H}_{\mathbf{k}} = \begin{pmatrix} \hat{H}_{\mathbf{k}}^{G,K} & 0 & \hat{T}^{\dagger} \\ 0 & \hat{H}_{\mathbf{k}}^{G,K'} & \hat{T}^{\dagger} \\ \hat{T} & \hat{T} & \hat{H}_{\mathbf{k}}^{TI} \end{pmatrix}, \quad \hat{\mathrm{T}} = \begin{pmatrix} t & 0 & 0 & 0 \\ 0 & 0 & t & 0 \end{pmatrix},$$
(1)

where $\hat{H}_{\mathbf{k}}^{G,K}$ ($\hat{H}_{\mathbf{k}}^{G,K'} = [\hat{H}_{\mathbf{k}}^{G,K}]^*$) is the Hamiltonian

describing the SLG's, $\hat{H}^{SLG,K}$ (BLG's $\hat{H}^{BLG,K}$) low energy states around the K (K') of the Brillouin zone. $\hat{H}_{\mathbf{k}}^{TI}$ is the Hamiltonian describing the TI's surface states, and $\hat{T}$ is the matrix describing spin- and momentum- conserving tunneling processes between the graphene layer and the TI's surface [4], t being the tunneling strength. The TI's bulk states are assumed to be gapped. This condition is realized, for example, in novel ternary or quaternary tetradymites, such as Bi_2Te_2Se and $Bi_{2-x}Sb_xTe_{3-y}Se_y$, for which it has been shown experimentally that the bulk currents have been completely eliminated [35–42]. For SLG we have $\hat{H}_{\mathbf{k}}^{SLG,K} = \hbar v_g k \sigma_0 [\cos(\phi_{\mathbf{k}})\tau_x + \sin(\phi_{\mathbf{k}})\tau_y] - \mu_g$, where $v_g \approx 10^6$ m/s is the graphene's Fermi velocity, $k = |\mathbf{k}|$, $\phi_{\mathbf{k}} = \arctan(k_y/k_x)$, σ_i, τ_i are the Pauli matrices in spin and sublattice space respectively, and μ_g is the chemical potential. For BLG we have $\hat{H}_{\mathbf{k}}^{BLG,K} = \hbar^2 k^2/(2m^*)\sigma_0 [\cos(2\phi_{\mathbf{k}})\tau_x + \sin(2\phi_{\mathbf{k}})\tau_y] - \mu_g$, where $m^* \approx 0.035 m_e$ is the effective mass. For the TI's surface states, we have $\hat{H}_{\mathbf{k}}^{TI} = \hbar v_{TI} (k_y \sigma_x - k_x \sigma_y) - \mu_{TI}\sigma_0$, where $v_{TI} \approx v_g/2$ and μ_{TI} is the chemical potential on the TI's surface . In the remainder the Fermi energy ϵ_F is measured from the neutrality point of the SLG (or the BLG) and $\delta\mu \equiv \mu_{TI} - \mu_g$.

In a magnetically doped TI, below the Curie temperature, the low energy Hamiltonian for the TI-graphene's quasiparticles, Eq. (1), has an additional term, H_{ex}, describing the exchange interaction between the quasiparticles and the magnetization $\mathbf{M}$. $H_{ex} = \Delta \int_{\Omega} \hat{\mathbf{m}} \cdot \hat{\mathbf{s}} \, d\mathbf{r}/\Omega$, where Δ is the strength of the exchange interaction, $\hat{\mathbf{m}} \equiv \mathbf{M}/|\mathbf{M}|$, $\hat{\mathbf{s}} \equiv \mathbf{s}/|\mathbf{s}|$ with $\mathbf{s}$ the TI-graphene's spin-density operator, and Ω is the 2D area of the sample. For a TI-graphene-ferromagnet heterostructure the ferromagnet (FM) will also cause simply the addition of the term H_{ex} to the Hamiltonian for the quasiparticles, Eq. (1), as long as the FM is an insulator, as is the case for the recently studied $Bi_2Se_3 - EuS$ systems [43, 44]. In the remainder, for TI-graphene-FM heterostructures we assume the FM to be an insulator.

To maximize the effect of the current-induced spin accumulation on the dynamics of the magnetization, it is ideal to have $\mathbf{M}$ perpendicular to the TI's surface. This is the case for magnetically doped TIs such as $Cr_{2x}(Bi_{0.5}Sb_{0.5-x})_2Te_3$ [18]. For TI-graphene-FM trilayers this can be achieved, for example, by using a thin film of $BaFe_{12}O_{19}$, a magnetic insulator with high T_c and large perpendicular anisotropy [45]. In the remainder we will assume $\hat{\mathbf{m}} = \hat{z}$.

By comparing the bands for TI-SLG, at low-energies, obtained from Eq. (1), Fig. 1 (d), with the ones obtained using DFT [27, 33, 34] we obtain that the effective value of t is ~ 45 meV. For this reason, most of the results that we show in the remainder were obtained assuming $t = 45$ meV. In the supplementary material (SM) we also consider different values of t, see Fig. 4 in the

SM. Fig. 1 (d) clearly shows that, in general, the hybridization of the graphene's and TI's states preserves a TI-like band and induces the formation of spin-splitted Rashba bands. The TI and Rashba nature of the bands can clearly be evinced from the winding of the spins, as shown in Fig. 1 (f). The same qualitative features can be observed in Fig. 1 (e) that shows the low energy bands of a TI-BLG system with $\Delta = 20$ meV, and $\delta\mu = 0$.

In the remainder, we restrict our analysis to the case in which ϵ_F is such that the system is metallic. In this case contributions to the SOT from interband-transitions [46] can be neglected and the SOT is primarily field-like. For most of the conditions of interest, quantum interference effects can be assumed to be negligible due to dephasing effects at finite temperatures and the large dimensionless conductance of the system. The SOT can be obtained by calculating the current-induced spin-density response function $\chi^{s_i J_j}(\mathbf{q}, \omega)$ that, within the linear response regime, is equal to the spin-current correlation function.

The unavoidable presence of disorder induces a broadening of the quasiparticle states, and vertex corrections that are captured by the diagrams shown in Fig. 1 in the SM [47]. In TIs charge impurities appear to be the dominant source of disorder [48] and so it is expected that they will also be in TI-graphene heterostructures. We therefore model the disorder as a random potential created by an effective 2D distribution of uncorrelated charge impurities with zero net charge placed at an effective distance d below the TI's surface. Direct imaging experiments [49] suggest $d \approx 1$ nm, consistent with transport results [48, 50].

In momentum space, the bare potential $v(q)$ created on the TI's surface by a single charge impurity is $v(q) = 2\pi e^2 e^{-qd}/(\kappa q)$ where $\kappa = (\kappa_{TI} + \kappa_0)/2$ is the average dielectric constant with $\kappa_{TI} \approx 100$ [48–52] the dielectric constant for the TIS and $\kappa_0 = 1$ the dielectric constant of vacuum [53]. The screened disorder potential is $v(q)/\epsilon(q)$ where $\epsilon(q)$ is the dielectric function [22, 54, 55]. To obtain the current-driven SOT in the dc limit, and for temperatures T much lower than the Fermi temperature T_F, to very good approximation we can assume $\epsilon(q) \approx 1 + v_c(q)\nu(\epsilon_F)$, where $v_c(q) = 2\pi e^2/(\kappa q)$ and $\nu(\epsilon_F)$ is the density of states at the Fermi energy.

The lifetime $\tau_{0a}(\mathbf{k})$ of a quasiparticle in band a with momentum $\mathbf{k}$ is given by

$$\frac{\hbar}{\tau_{0a}(\mathbf{k})} = 2\pi \sum_{a'\mathbf{q}} n_{\text{imp}} \left| \frac{v(q)}{\epsilon(q)} \right|^2 |\langle a'\mathbf{k+q}|a\mathbf{k}\rangle|^2 \delta(\epsilon_{a,\mathbf{k}} - \epsilon_{a',\mathbf{k+q}}),$$

(2)

where n_{imp} is the impurity density and $|a\mathbf{k}\rangle$ is the Bloch state with momentum $\mathbf{k}$ and band index a. In the remainder, we set $n_{\text{imp}} = 10^{12}\text{cm}^{-2}$ [48]. The transport time $\tau_{ta}(\mathbf{k})$, that renormalizes the expectation value of the velocity operator, is obtained by introducing the factor $[1 - \mathbf{k} \cdot (\mathbf{k} + \mathbf{q})]$ under the sum on the right hand

side of Eq. (2), and in general differs from the lifetime $\tau_{0a}(\mathbf{k})$ [56–60]. We define the average τ_0, τ_t as $\langle \tau_{0(t)}(\epsilon_F) \rangle \equiv \sum_{\mathbf{k}a} \tau_{0a(ta)}(\mathbf{k}) \delta(\epsilon_F - \epsilon_{\mathbf{k}a}) / \sum_{\mathbf{k}a} \delta(\epsilon_F - \epsilon_{\mathbf{k}a})$. Figs. 2 (a), (b) show $\langle \tau_0(\epsilon_F) \rangle$, and $\langle \tau_t(\epsilon_F) \rangle$, respectively, for a TI's surface, a TI-SLG heterostructure, and a TI-BLG heterostructure, with $\Delta = 0$ meV. We see that the presence of a graphene layer strongly increases both $\langle \tau_0(\epsilon_F) \rangle$, and $\langle \tau_t(\epsilon_F) \rangle$, and that such increase is dramatic for the case when the layer is BLG. $\langle \tau_0(\epsilon_F) \rangle$, and $\langle \tau_t(\epsilon_F) \rangle$ are larger in BLG-TI than TI-SLG because, especially at low energies, BLG has a larger density of states than SLG causing $\varepsilon(q)$, that enters in the denominator in Eq. (2), and therefore $\langle \tau_0(\epsilon_F) \rangle$, and $\langle \tau_t(\epsilon_F) \rangle$ to be larger in BLG than in SLG. Notice that τ_0, τ_t increase after adding a graphene layer even in the limit when $t = 0$ as shown by the dashed lines in Fig. 2. This is due to the fact that the graphene layer screens the dominant source of disorder in the TI even when $t = 0$. Changes in Δ have only minor quantitative effects as long as $\Delta < (t, \epsilon_F)$.
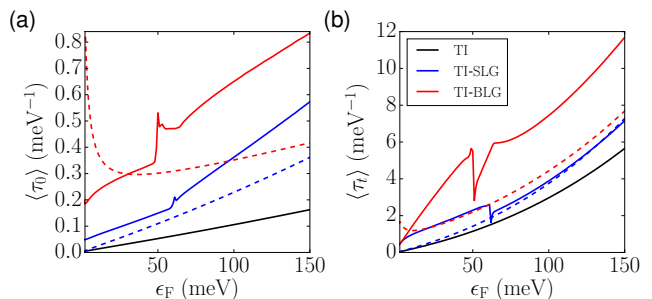

FIG. 2: $\langle \tau_0(\epsilon_F) \rangle$, (a), and $\langle \tau_t(\epsilon_F) \rangle$, (b) for $\Delta = 0 = \delta\mu = 0$, and $n_{\text{imp}} = 10^{12}$ cm^{-2}. The dashed lines show the results for the limit $t = 0$, the solid one the ones for $t = 45$ meV.

For a charge current in the y direction the non equilibrium spin density is polarized in the x direction, as shown schematically in Fig. 3 (a). Due to the rotational symmetry of the system we have $\chi^{s_x J_y} = -\chi^{s_y J_x}$ and $\chi^{s_x J_x} = \chi^{s_y J_y}$. Without loss of generality we can assume the current to be in the y direction. In the long wavelength, dc, limit we have

$$\chi^{s_x J_y} \approx \frac{e}{2\pi\Omega} \text{Re} \sum_{\mathbf{k},a} s_{aa}^x(\mathbf{k}) \tilde{v}_{aa}^y(\mathbf{k}) G_{\mathbf{k}a}^A G_{\mathbf{k}a}^R, \quad (3)$$

where $s_{aa}^i(\mathbf{k}) \equiv \langle a\mathbf{k}|s_i|a\mathbf{k}\rangle$ is the expectation value of the i-th component of the spin-density operator, $\tilde{v}_{aa}^i(\mathbf{k}) = (\tau_a/\tau_{0a})_{\mathbf{k}} v_{aa}^i(\mathbf{k})$ with $v_{aa}^i(\mathbf{k}) \equiv \langle a\mathbf{k}|v_i|a\mathbf{k}\rangle$ the expectation value of the i-th component of the velocity operator $\mathbf{v} = \hbar^{-1}\partial H_{\mathbf{k}}/\partial \mathbf{k}$, and $G_{\mathbf{k}a}^{R/A} = (\epsilon_F - \epsilon_{\mathbf{k}a} \pm i\hbar/2\tau_{0a}(\mathbf{k}))^{-1}$ are the retarded and advanced Green's functions, respectively, for electrons with momentum $\mathbf{k}$ and band index a.

Figure 3 (b) shows the dependence of $\chi^{s_x J_y}$ on ϵ_F for TI, TI-SLG, and TI-BLG, assuming $t = 45$ meV, $\delta\mu = 0$ and $\Delta = 20$ meV ($\Delta = 0$) solid lines (dashed lines).
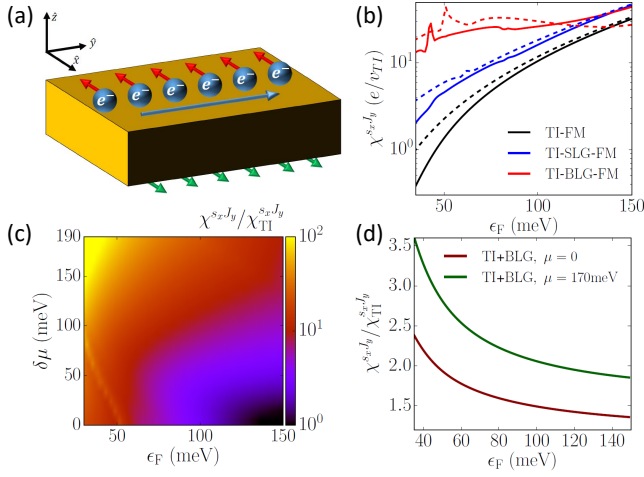
FIG. 3: (a) Sketch showing the spin density accumulation on the top and bottom surface of a TI induced by a current in the y direction. (b) $\chi^{s_x J_y}$ as a function of ϵ_F for $\delta\mu = 0$ and $\Delta = 20$ meV ($\Delta = 0$), solid (dashed) lines. (c) Enhancement of $\chi^{s_x J_y}$ in a TI-BLG system compared to TI alone as a function of ϵ_F and $\delta\mu$ for $\Delta = 0$. (d) $\chi^{s_x J_y}$ for TI-BLG when $t = 0$.

We see that the insertion of a graphene layer strongly enhances the current-induced spin density response and therefore the SOT. In addition, we find that the strong enhancement of $\chi^{s_x J_y}$ is not affected significantly by the value of Δ [47]. On the other hand, we find that changes in $\delta\mu$ have a strong impact on $\chi^{s_x J_y}$. Figure 3 (c) shows that by increasing $\delta\mu$ the enhancement of the SOT can be raised to values as high as 100 in TI-BLG heterostructures due to the flattening and consequent increase of the DOS of the TI-like bands [47].

The results of Fig. 3 show that in TI-SLG and TI-BLG heterostructures the current-induced SOT can be expected to be much higher than in TI surfaces alone. They show that for TI-BLG systems there is a large range of values of $\delta\mu$, ϵ_F for which the enhancement of $\chi^{s_x J_y}$ due to the presence of the BLG is consistently close to 10 or larger, Fig. 3 (c). In addition, in a TI-graphene heterostructure, by placing the source and drain on the graphene (BLG) and taking into account the high mobility of graphene (BLG), it is possible to force most of the current to flow within graphene (BLG) and the TI's surface adjacent to it. Therefore we can minimize the amount of spin-density accumulation with opposite polarization that a current flowing in the TI's bottom surface generates. This fact should further increase the net SOT.

The large enhancement of the SOT in TI-graphene systems is due to two main reasons: (i) the survival, after hybridization, of TI-like bands well separated from Rashba bands; (ii) the strong enhancement of the relaxation time τ_0 and transport time τ_t due to the additional screening by the graphene layer of the dominant source of disorder. It is important to notice that the presence of the

Rashba bands, see Fig. 1, not only is not essential for the enhancement of the SOT but it can be detrimental given that the Rashba bands give a SOT with opposite sign of the TI-like bands. This fact can be seen at large Fermi energies for BLG-TI in Fig. (3) (b): for $\epsilon_F \gtrsim 140$ meV the Fermi surface intersect the Rashba bands that by giving a SOT opposite to the TI-like bands brings the net SOT of TI-BLG to be slightly lower than the SOT of TI-alone. Point (ii) explains the fact the SOT, at low energies, is always larger in TI-BLG rather than TI-SLG given that τ_0 and τ_t are larger in TI-BLG than in TI-SLG. In addition, it explains the fact that even in the limit when there is no hybridization between the TI and the graphene bands, i.e. t=0, (due for example to a large twist angle [47]) the SOT in TI-graphene systems is still larger than in TIs alone as shown in Fig. 3 (d).
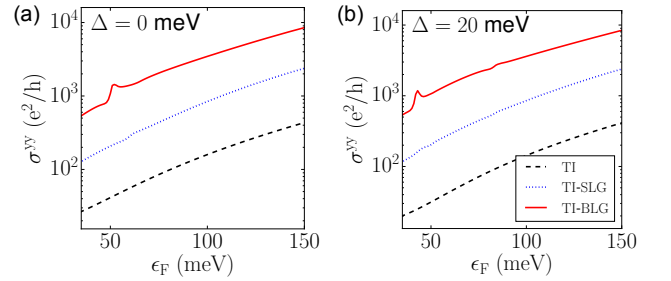

FIG. 4: $\sigma^{yy}(\epsilon_F)$, for TI (dashed line), TI-SLG (dotted line), and TI-BLG (solid line) for $\Delta = 0$, (a), and $\Delta = 20$ meV (b). $t = 45$ meV, $\delta\mu = 0$, and $n_{\text{imp}} = 10^{12}$ cm^{-2}.

To estimate the efficiency of the current-induced SOT in TI-graphene heterostructure we calculate the associated dc longitudinal conductivity σ^{ii} for the same parameters. In the linear-response, long-wavelength, regime we have

$$\sigma^{ii} \approx \frac{e^2}{2\pi\Omega} \text{Re} \sum_{\mathbf{k},a} v_{aa}^i(\mathbf{k}) \tilde{v}_{aa}^i(\mathbf{k}) G_{\mathbf{k}a}^A G_{\mathbf{k}a}^R . \quad (4)$$

Fig. 4 (a) shows σ^{yy} for TI, TI-SLG, and TI-BLG as a function of ϵ_F in the limit $\Delta = 0$. We see that the presence of a graphene layer enhances the conductivity of the system by an order of magnitude or more. Fig. 4 (b) shows that the exchange term H_{ex} does not affect σ^{yy} significantly. The results shown in Fig. 4 (b) imply that in TI-graphene heterostroctures not only the current-induced SOT can be much larger than in TIs alone, but also that the generation of the SOT is much less dissipative.

In conclusion, we have shown that in magnetic TI-graphene heterostructures the non-equilibrium uniform spin density accumulation induced by a charge current can be 10-100 times higher than in TIs alone giving rise to a giant SOT. The reasons for these enhancements are (i) the additional screening by the graphene layer of the dominant source of disorder; (ii) the fact that graphene

and the TI's surface are almost commensurate making possible a strong hybridization of the TI's and graphene's states; (iii) the fact that the spin structure of the hybridized bands has a spin structure very similar to the one of the original TI's band for a large range of dopings; (iv) the fact that graphene is the ultimate 2D system, only one-atom thick. These facts and our results suggest the TI-graphene systems are very good candidates to realize all-electric efficient magnetization switching.

[1] I. Žutić, J. Fabian, and S. Das Sarma, Rev. Mod. Phys. **76**, 323 (2004).

[2] J. Sinova, S. O. Valenzuela, J. Wunderlich, et al., Rev. Mod. Phys. **87**, 1213 (2015).

[3] M. Z. Hasan and C. L. Kane, Rev. Mod. Phys. **82**, 3045 (2010).

[4] X.-L. Qi and S.-C. Zhang, Rev. Mod. Phys. **83**, 1057 (2011).

[5] J. Sinova and I. Žutić, Nature Materials **11**, 368 (2012).

[6] A. Brataas, A. D. Kent, and H. Ohno, Nature Materials **11**, 372 (2012).

[7] T. Jungwirth, J. Wunderlich, and K. Olejník, Nature Materials **11**, 382 (2012).

[8] G. E. W. Bauer, E. Saitoh, and B. J. van Wees, Nature Materials **11**, 391 (2012).

[9] M. Dyakonov and V. Perel, Physics Letters A **35**, 459 (1971).

[10] V. Edelstein, Solid State Communications **73**, 233 (1990).

[11] M. I. Dyakonov (Ed.), *Spin physics in semiconductors*, vol. 157 of *Springer Series in Solid-State Sciences* (Springer, New York, 2008).

[12] H. Kurebayashi et al., Nature Nanotechnology **9**, 211 (2014).

[13] I. Garate and M. Franz, Phys. Rev. Lett. **104**, 146802 (2010).

[14] T. Yokoyama, J. Zang, and N. Nagaosa, Phys. Rev. B **81**, 241410 (2010).

[15] A. Sakai and H. Kohno, Phys. Rev. B **89**, 165307 (2014).

[16] M. H. Fischer, A. Vaezi, A. Manchon, and E.-A. Kim, Phys. Rev. B **93**, 125303 (2016).

[17] A. R. Mellnik et al., Nature **511**, 449 (2014).

[18] Y. Fan et al., Nature Nanotechnology **11**, 352 (2016).

[19] K. S. Novoselov et al., Nature **438**, 197 (2005).

[20] Y. Zhang et al., Nature **438**, 201 (2005).

[21] A. H. C. Neto et al., Rev. Mod. Phys. **81**, 109 (2009).

[22] S. Das Sarma et al., Rev. Mod. Phys. **83**, 407 (2011).

[23] K. Vaklinova et al., Nano Letters **16**, 2595 (2016).

[24] J. Tian et al., ArXiv **1607.02651** (2016).

[25] In both experiments the currents are AC and the values provided in the text are the r.m.s. values. In the setup used in Ref. [17] a big fraction of the current flows through the bulk of the TI and the ferromagnetic metal (Py) placed on top of the TI, whereas in the setup used in Ref. [18], in optimal conditions, most of the current flows through the TI's surfaces.

[26] S. J. Haigh et al., Nature Materials **11**, 764 (2012).

[27] K.-H. Jin and S.-H. Jhi, Phys. Rev. B **87**, 075442 (2013).

[28] J. R. Wallbank, M. Mucha-Kruczyński, and V. I. Fal'ko, Phys. Rev. B **88**, 155415 (2013).

[4] J. Zhang, C. Triola, and E. Rossi, Phys. Rev. Lett. **112**, 096802 (2014).

[30] H. Steinberg et al., Phys. Rev. B **92**, 241409 (2015).

[31] G. Bian et al., 2D Materials **3**, 021009 (2016).

[32] L. A. Ponomarenko et al., Nature **497**, 594 (2013).

[33] P. Lee, K.-H. Jin, S. J. Sung, et al., ACS Nano **9**, 10861 (2015).

[34] S. Rajput, Y.-Y. Li, M. Weinert, and L. Li, ACS Nano **10**, 8450 (2016).

[35] Z. Ren, A. A. Taskin, S. Sasaki, K. Segawa, and Y. Ando, Phys. Rev. B **82**, 241306 (2010).

[36] J. Xiong, A. C. Petersen, D. X. Qu, Y. S. Hor, R. J. Cava, and N. P. Ong, Physica E **44**, 917 (2012).

[37] T. Arakane, T. Sato, S. Souma, K. Kosaka, K. Nakayama, M. Komatsu, T. Takahashi, Z. Ren, K. Segawa, and Y. Ando, Nature Comm. **3**, 636 (2012).

[38] B. Xia, P. Ren, A. Sulaev, P. Liu, S. Q. Shen, and L. Wang, Phys. Rev. B **87**, 085442 (2013).

[39] K. Segawa, Z. Ren, S. Sasaki, T. Tsuda, S. Kuwabata, and Y. Ando, Phys. Rev. B **86**, 075306 (2012).

[40] Y. Xu, I. Miotkowski, C. Liu, J. Tian, H. Nam, N. Alidoust, J. Hu, C.-K. Shih, M. Z. Hasan, and Y. P. Chen, Nature Physics **10**, 956 (2014).

[41] C. Durand, X.-G. Zhang, S. M. Hus, C. Ma, M. A. McGuire, Y. Xu, H. Cao, I. Miotkowski, Y. P. Chen, and A.-P. Li, Nano Letters **16**, 2213 (2016).

[42] Y. Xu, I. Miotkowski, and Y. P. Chen, Nat Commun **7** (2016).

[43] C. Lee et al., Nature Communications **7**, 12014 (2016).

[44] F. Katmis et al., Nature **533**, 513 (2016).

[45] W. Yang et al., Applied Physics Letters **105**, 092411 (2014).

[46] N. A. Sinitsyn et al., Phys. Rev. B **75**, 045315 (2007).

[47] Supplementary material. (2016).

[48] D. Kim et al., Nature Physics **8**, 459 (2012).

[49] H. Beidenkopf et al., Nat Phys **7**, 939 (2011).

[50] Q. Li, E. Rossi, and S. Das Sarma, Phys. Rev. B **86**, 235443 (2012).

[51] D. Culcer et al., Phys. Rev. B **82**, 155457 (2010).

[52] N. P. Butch et al., Phys. Rev. B **81**, 241301 (2010).

[53] Strictly speaking the value $\kappa_0 = 1$ is only valid for the case of a magnetically doped TI. However, given the large static dielectric constant of the TI, the error made by approximating the FM's dielectric constant by the vacuum's is negligible. For EuS, the suggested insulating FM, $\kappa_0 \approx 10$ giving an effective average dielectric constant $\kappa = 55$, instead of the used $\kappa = 50$. .

[54] E. H. Hwang, S. Adam, and S. Das Sarma, Phys. Rev. Lett. **98**, 186806 (2007).

[55] C. Triola and E. Rossi, Phys. Rev. B **86**, 161408 (2012).

[56] S. Das Sarma and F. Stern, Phys. Rev. B **32**, 8442 (1985).

[57] K. Nomura and A. H. MacDonald, Phys. Rev. Lett. **98**,

076602 (2007).

[58] E. Rossi and S. Das Sarma, Phys. Rev. Lett. **101**, 166803 (2008).

[59] E. Rossi, S. Adam, and S. D. Sarma, Phys. Rev. B **79**, 245423 (2009).

[60] C.-P. Lu et al., PNAS **113**, 6623 (2016).

SUPPLEMENTARY MATERIAL FOR "GIANT SPIN-ORBIT TORQUE IN GRAPHENE–TOPOLOGICAL-INSULATOR HETEROSTRUCTURES"

TI-BLG band structure

As long as the interlayer tunneling t_{BLG} between the carbon atoms in bilayer graphene is much larger than the expected tunneling t between the TI's surface and the graphenic layer any difference between the tunneling strength between the carbon layers forming BLG and the TI will give very negligible effects. Considering that in bilayer graphene the interlayer tunneling is 350 meV, and the fact that for the graphene-TI tunneling t we only consider values smaller than 45 meV for all our results is $t \ll t_{BLG}$. In this limit, at low energies ($\lesssim 350$ meV), BLG can be treated as 2D system with the effective Hamiltonian H^{BLG} presented in the main text.

Fig. 1 (e) in the main text shows the bands of a TI-BLG systems for which the exchange field $\Delta = 20$ meV and $\delta\mu = 0$. Fig 3 shows that the strongest enhancement of the SOT happens for TI-BLG systems when $\delta\mu \neq 0$. It is therefore interesting to see how the low-energy bands of TI-BLG are affected by a nonzero value of $\delta\mu$. Fig. 5 shows the band structure of TI-BLG for the case when $\delta\mu = 125$ meV in the absence of any exchange field. We see that one of TI-like bands (shown in orange) becomes much flatter: the high density of states of this band explains the high values of SOT for TI-graphene systems when $\delta\mu \neq 0$.
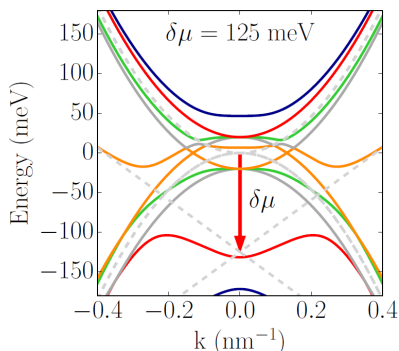
FIG. 5: TI-BLG band structure for $\delta\mu = 125$ meV, and tunneling amplitude $t = 45$ meV.

Feynman diagrams for the response function

Within the linear response regime, taking into account the presence of disorder, the response functions χ^{XY} of the system can be obtained by calculating the diagrams shown in Fig. (6). The diagram in Fig. (6a) represents the equation for the self-energy in the first Born approximation, where the double line represents the disorder-dressed electrons' Green's function, the single line the electron's Green's function for the clean system, and the dashed lines scattering events off the impurities. The diagram in Fig. (6b) corresponds to the equation for the renormalized vertex, $\tilde{Y}$, at the ladder level approximation. The diagram in Fig. (6c) corresponds to the response function χ^{XY}, which is given by

$$\chi^{XY} \approx \frac{1}{2\pi\Omega} \operatorname{Re} \sum_{\mathbf{k},a} X_{aa}(\mathbf{k}) \tilde{Y}_{aa}(\mathbf{k}) G_{\mathbf{k}a}^{A} G_{\mathbf{k}a}^{R} , \quad (5)$$

where $O_{aa}(\mathbf{k}) \equiv \langle a\mathbf{k}|O|a\mathbf{k}\rangle$, and $G_{\mathbf{k}a}^{R/A} = (\epsilon_F - \epsilon_{\mathbf{k}a} \pm i\hbar/2\tau_{0a}(\mathbf{k}))^{-1}$ are the retarded and advanced Green's functions respectively for electrons with momentum $\mathbf{k}$ and band index a.
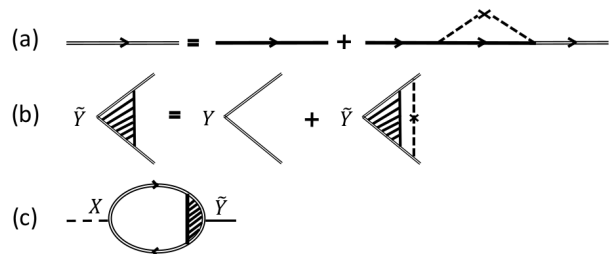
FIG. 6: Diagrams used to calculate the charge conductivity and the spin-current response.

Dependence on exchange interaction, tunneling amplitude, and effective impurity distance of the inverse spin-galvanic effect

In Fig. (7) we show the current-induced spin density accumulation response function as a function of the exchange interaction between the FM and the TI-graphene heterostructure. Panel (a) shows the case of the TI-FM heterostructure, and panel (b) shows the ratio of a TI-BLG(SLG)-FM heterostructure response to the TI-FM response at $\epsilon_F = 60$ meV.

In Fig. (8) we plot the current-induced spin density accumulation response function as a function of the tunneling amplitude t between graphene and the TI, normalized to the TI response function. As t is increased, TI and graphene hybridize more strongly, leading to a larger response. In the main text, we fix $t = 45$ meV.

In Fig. (9) we plot the current-induced spin density accumulation response function as a function of the effective distance to the impurities d. The further away the impurities are located, the weaker the disorder, and the larger the response. In the main text we fix $d = 1$ nm.
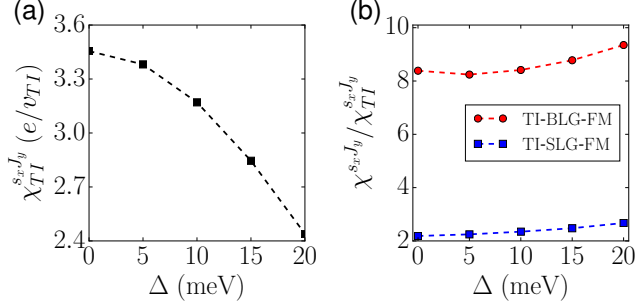

FIG. 7: (a) $\chi^{s_x J_y}$ as a function of the exchange interaction Δ for a TI-FM heterostructure at $\epsilon_F = 60$ meV. (b) Ratio $\chi^{s_x J_y}/\chi^{s_x J_y}_{TI}$ of the TI-BLG-FM (red circles) and TI-SLG-FM (blue squares) response to the TI-FM response.
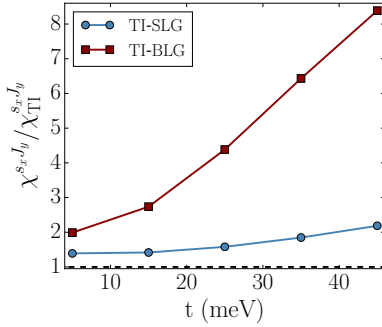

FIG. 8: $\chi^{s_x J_y}$ as a function of the tunneling amplitude t for TI-SLG and TI-BLG heterostructures at $\epsilon_F = 60$ meV.
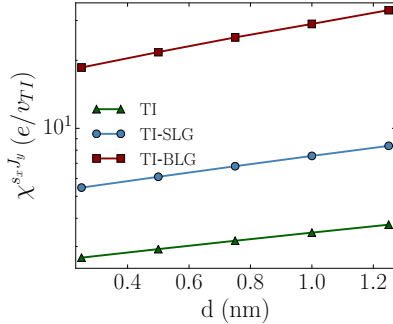

FIG. 9: $\chi^{s_x J_y}$ as a function of the effective distance to the impurities d for TI-SLG and TI-BLG heterostructures at $\epsilon_F = 60$ meV.

Inverse spin galvanic effect in twisted TI-graphene heterostructures

It can expected that even when the stacking of the graphenic layer and the TI's surface is incommensurate, the screening of the charge impurities by the graphenic layer will lead to a strong enhancement of τ_0 and τ_t and therefore of the SOT. The accurate treatment of the realistic case in which the main source of disorder are charge impurities for incommensurate stackings requires the calculation of the dielectric constant for incommensurate structures, a task that is beyond the scope of the present work. For this reason, to exemplify how the presence of a small twist angle θ between the graphenic layer and the TI surface, giving rise to an incommensurate stacking, affects the calculation of the SOT, we consider a very simple model for the effect of the disorder: we simply assume that the disorder gives rise to a constant quasiparticle broadening.

Let $|\mathbf{q}| \equiv q = 2K_D \sin(\theta/2)$, where K_D is the magnitude of the graphene K point. The dimensionless parameter $\gamma \equiv \frac{t'}{\hbar v_{TI} q}$, where $t' = t/3$, measures the strength of the coupling between the graphenic layer and the TIS. For $\gamma < 1$ we can obtain the electronic structure using the weak coupling theory for twisted systems [1–3] that for the case of a TI-graphene heterostructures we presented in Ref. [4]. After obtaining the electronic structure in the regime $\gamma < 1$, we can obtain $\chi^{s_x J_y}$. To understand how the response between the commensurate and the incommensurate regimes differ, we have calculated $\chi^{s_x J_y}$ assuming a constant quasiparticle broadening $1/(2\tau_0) = 2$ meV, with $t' = 15$ meV, $\delta\mu = 0$, and $\epsilon_F = 10$ meV for a range of values of θ for which the weak coupling theory is valid. The dependence of $\chi^{s_x J_y}$, per valley, as a function of θ for TI-SLG and TI-BLG is shown in Fig. 10. As to be expected, the results show that in the incommensurate case the response is smaller than in the commensurate case. However, they also show, in particular for the case in which the graphenic layer is BLG, that a TI-graphene heterostructure is expected to have stronger $\chi^{s_x J_y}$, and therefore a stronger inverse spin-galvanic effect, even in the incommensurate regime and for the case in which the disorder is modeled very simply.

[1] J. Lopes dos Santos, N. Peres, and A. Castro Neto, Phys. Rev. Lett. **99**, 256802 (2007).
[2] R. Bistritzer and A. H. MacDonald, Proc. National Acad. Sciences United States Am. **108**, 12233 (2011).
[3] E. J. Mele, Journal of Physics D Applied Physics **45**, 154004 (2012).
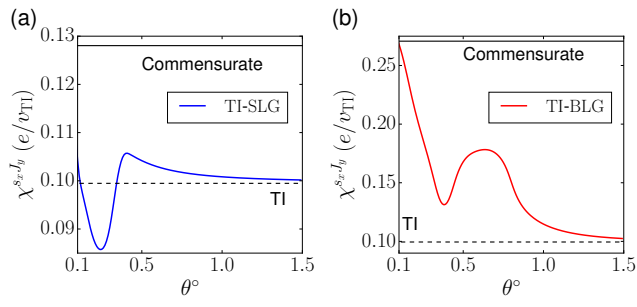[4] J. Zhang, C. Triola, and E. Rossi, Phys. Rev. Lett. **112**, 096802 (2014).

FIG. 10: (a) $\chi^{s_x J_y}$ as a function of twist angle θ for TI-SLG. (b) Same as (a) for TI-BLG.